Research Article

Zhan Guo, Qingxia Zhu, Wenda Wu, and Yu Chen*

Research on bond–slip performance between pultruded glass fiber-reinforced polymer tube and nano-$CaCO_3$ concrete

https://doi.org/10.1515/ntrev-2020-0036
received March 23, 2020; accepted April 01, 2020

Abstract: The article describes an experimental study on the bond–slip performance between the pultruded glass fiber-reinforced polymer (GFRP) tube and the nano-$CaCO_3$ concrete. Taking the nano-$CaCO_3$ concrete strength and GFRP tube thickness as primary parameters, nine specimens were designed and tested to study the influence of these parameters on the bond strength of the specimens. Besides, three specimens filled with the ordinary concrete were also tested by using the push-out tests to make comparisons with the bond performance of the specimens filled with nano-$CaCO_3$ concrete. A total of four push-out tests were conducted on each specimen. The experimental results indicate that there are two types of axial load–slip curves for each specimen in four push-out tests. Moreover, comparison of the results of the push-out tests in the same direction shows that the bond failure load of the specimen decreases with the increase in the number of push-out tests. Based on the analysis of the test results, it is shown that the bond performance between the GFRP tube and the nano-$CaCO_3$ concrete is better than that between the GFRP tube and the ordinary concrete. Furthermore, as the nano-$CaCO_3$ concrete strength increases, the bond strength of the specimens decreases, indicating that the concrete strength has a negative effect on the bond strength. When the nano-$CaCO_3$ concrete strength is relatively smaller (C20), the bond strength of the specimens decreases with the increase in the thickness of the GFRP tube. However, when the nano-$CaCO_3$ concrete strength is relatively larger (C30 and C40), the bond strength of the specimens increases as the thickness of the GFRP tube increases.

Keywords: bond–slip performance, bond strength, nano-$CaCO_3$ concrete, pultruded GFRP tube, push-out tests

1 Introduction

In recent years, with the rapid development of nanotechnology, more and more nanomaterials have been developed. Because of their excellent characteristics, nanomaterials are widely applied in various fields [1–4]. Therefore, nanomaterials have been studied in various fields, including construction materials, medicine, environment, and chemistry. It is well known that concrete is one of the most extensively used construction materials in the field of civil engineering. Hence, many research studies were performed on the concrete mixed with nanomaterials, and these research studies explained that nanomaterials could effectively improve the physical and chemical properties of concrete [5–9]. Guo et al. [10] discussed the effect of GO nanomaterials on the chloride penetration resistance of the recycled concrete. Their findings indicated that the incorporation of GO nanomaterials could significantly improve the chloride penetration resistance of the recycled concrete. Pacheco-Torgal et al. [11] indicated that the addition of nanoparticles to the concrete aggregates could significantly improve the strength and durability of the concrete. Lin et al. [12] experimentally investigated the mechanical behavior of the circular nano-silica concrete-filled stainless steel tubular columns after exposure to freeze–thaw cycles. Their test results showed that the freeze–thaw cycles had a significant influence on the residual load-bearing capacity of the nano-silica concrete-filled columns. He et al. [13] reported that the increase in the compressive strength of the nano-silica concrete could effectively enhance the bearing capacity and initial stiffness of the glass fiber-reinforced polymer (GFRP) composite columns. Behfarnia et al. [14] experimentally investigated

* **Corresponding author: Yu Chen,** College of Civil Engineering, Fuzhou University, Fuzhou, 350116 China,
e-mail: kinkingingin@163.com, tel: +86 18030219629
Zhan Guo, Wenda Wu: College of Civil Engineering, Fuzhou University, Fuzhou, 350116 China
Qingxia Zhu: School of Urban Construction, Yangtze University, Jingzhou, 434023 China

Open Access. © 2020 Zhan Guo *et al.*, published by De Gruyter. This work is licensed under the Creative Commons Attribution 4.0 Public License.

the mechanical behaviour and frost resistance of concrete containing nanomaterials after being subjected to freeze-thaw cycles. They found that the frost resistance and microstructure of concrete containing nano-particles were significantly improved. Especially, due to the stable performance and low price of nano-$CaCO_3$, it has become a perfect additive in construction materials. Adding an appropriate amount of nano-$CaCO_3$ into concrete can improve the strength, frost resistance, and durability of concrete. Shaikh and Supit [15] showed that the addition of nano-$CaCO_3$ could obviously improve the durability of concrete. Shaikh and Supit [16] also found that the compressive strength of the concrete with 1% nano-$CaCO_3$ was the highest; its early compressive strength was about 146% higher than that of the ordinary concrete, and its compressive strength at 90 days was about 40% higher than that of the ordinary concrete. Besides, the research results of Liu et al. [17] showed that the addition of nano-$CaCO_3$ could shorten the setting time of cement, reduce the fluidity of mixture, and accelerate the hydration reaction rate of cement.

The concrete-filled GFRP column is a new type of composite structure initially proposed by Mirmiran et al. [18,19]. In this novel composite structure, the fresh concrete is poured into the GFRP tube, and the external GFRP tube can be used as the formwork of the structure. This can avoid the tedious process of making formwork and removing formwork, thereby saving time and shortening the construction period. The external GFRP tube can also constrain the core concrete and improve the load-carrying capacity of the core concrete [20]. At the same time, the external GFRP tube also plays a role similar to the hooping in the reinforced concrete columns, which can improve the shear carrying capacity of the inclined section of the column. Moreover, the core concrete can prevent the local buckling of the external GFRP tube, thus enhancing the structural stability [21]. The GFRP composite materials also have the characteristics of lightweight and corrosion resistance [22–26]. Therefore, the GFRP tube can protect the core concrete and improve the overall durability of structures when they are used in a relatively harsh environment. The above relevant studies show that the nano-$CaCO_3$ concrete has better mechanical performance and durability than the ordinary concrete. Therefore, it can be an innovative idea that the nano-$CaCO_3$ concrete was used to fill the GFRP tube in practical engineering. When the nano-$CaCO_3$ is added into the ordinary concrete, the bond performance between the core concrete and the GFRP tube might be significantly enhanced owing to the tiny structural unit of nano-$CaCO_3$. However, the research on the bond–slip performance is mainly focused on the ordinary concrete and FRP materials.

Gooranorimi et al. [27] established the bond–slip model of the GFRP bars and concrete. It was found that the model could reflect the failure mode of concrete. Gooranorimi et al. [28] also studied the bond–slip relationship between the FRP and the reinforced concrete. Yuan et al. [29] conducted an experiment to investigate the bond–slip behavior of the FRP–concrete interface. In addition, Vilanova et al. [30] performed a numerical simulation of bond–slip between the FRP and the reinforced concrete. According to the test results and the finite element results, Tekle et al. [31] found that the distribution of bond stress between the GFRP bars and the alkali-activated cement was nearly uniform. An experimental study was performed by Yuan and Hadi [32] to study the bond–slip performance between concrete and I-section GFRP. Moreover, the bond stress–slip model was established and validated by comparison with the experimental results. Based on the existing bond strength models, Lu et al. [33] proposed a series of new bond–slip models by the combination of the finite element results and the test results. These models were recommended for future use in the numerical modeling of the FRP-strengthened reinforced concrete structures.

To develop a composite action, the GFRP tube and concrete should have superior bond between them. Although many researchers have investigated the bond–slip performance between the ordinary concrete and the FRP materials, little experimental study and theoretical analysis have been carried out on the bond–slip performance between the nano-$CaCO_3$ concrete and the GFRP tube. In this study, the nano-$CaCO_3$ particles are added to the ordinary concrete to study the bond–slip performance between the GFRP and the nano-$CaCO_3$ concrete. In particular, the effects of nano-$CaCO_3$ concrete strength and thickness of the GFRP tube on the bond strength of the specimens are analyzed and evaluated systematically. This article can provide a good reference for further relevant research studies and contribute to the practical application of nano-$CaCO_3$ concrete-filled GFRP structures in the engineering construction fields.

2 Experimental program

2.1 Test specimens

A total of 12 specimens were designed and tested in this experiment, including three specimens filled with the ordinary concrete and nine specimens filled with the nano-$CaCO_3$ concrete. The bond–slip performance between the pultruded GFRP tube and the nano-$CaCO_3$

concrete was experimentally studied, and the effects of nano-$CaCO_3$ concrete strength and GFRP tube thickness on the bond strength of the specimens were analyzed. Besides, the bond performance between the GFRP tube and the nano-$CaCO_3$ concrete was also compared with that between the GFRP tube and the ordinary concrete. Three kinds of nano-$CaCO_3$ concrete with different concrete strengths (C20, C30, and C40) were prepared, and the thickness of the GFRP tube also has three different grades, ranging from 3.5 to 5.0 mm. In this experiment, the cross-section dimension ($b \times b$) of the pultruded GFRP tube is 100 mm × 100 mm, and the height (h) of the GFRP tube is uniformly 250 mm. To conduct four repeated push-out tests on each specimen, it is necessary to leave a gap of 30 mm at the top of each specimen. Pictures of the prepared specimen are shown in Figure 1. Table 1 shows the detailed parameters of the test specimens. As shown in Table 1, all specimens are named according to the nano-$CaCO_3$ concrete strength and the GFRP tube thickness. For example, the label "GT3.5-C20" of the specimen is defined as follows:

- "GT3.5" represents that the thickness of the pultruded GFRP tube is 3.5 mm.
- "C20" indicates that the nano-$CaCO_3$ concrete strength is C20. In particular, "OC20" indicates that the ordinary concrete strength is C20.

Table 1: Parameters of test specimens

Specimens	h (mm)	b (mm)	T (mm)	h/b	b/T	f_{cu} (MPa)
GT3.5-C20	250	100	3.5	2.5	28.6	20
GT3.5-C30	250	100	3.5	2.5	28.6	30
GT3.5-OC30	250	100	3.5	2.5	28.6	30
GT3.5-C40	250	100	3.5	2.5	28.6	40
GT4.0-C20	250	100	4.0	2.5	25.0	20
GT4.0-C30	250	100	4.0	2.5	25.0	30
GT4.0-OC30	250	100	4.0	2.5	25.0	30
GT4.0-C40	250	100	4.0	2.5	25.0	40
GT5.0-C20	250	100	5.0	2.5	20.0	20
GT5.0-C30	250	100	5.0	2.5	20.0	30
GT5.0-OC30	250	100	5.0	2.5	20.0	30
GT5.0-C40	250	100	5.0	2.5	20.0	40

2.2 Material properties

The material properties of the pultruded GFRP tube are determined by standard tensile tests. Because of the anisotropy of the material, transverse and longitudinal tensile tests are required. The tensile tests were performed in accordance with the ASTM D 3039 [34]. Table 2 shows the test results of the material property of the pultruded GFRP tube, including the elastic modulus (E_G), yield strength (f_{yG}), tensile strength (f_{uG}), average yield strength (f_{ay}), and average tensile strength (f_{au}).

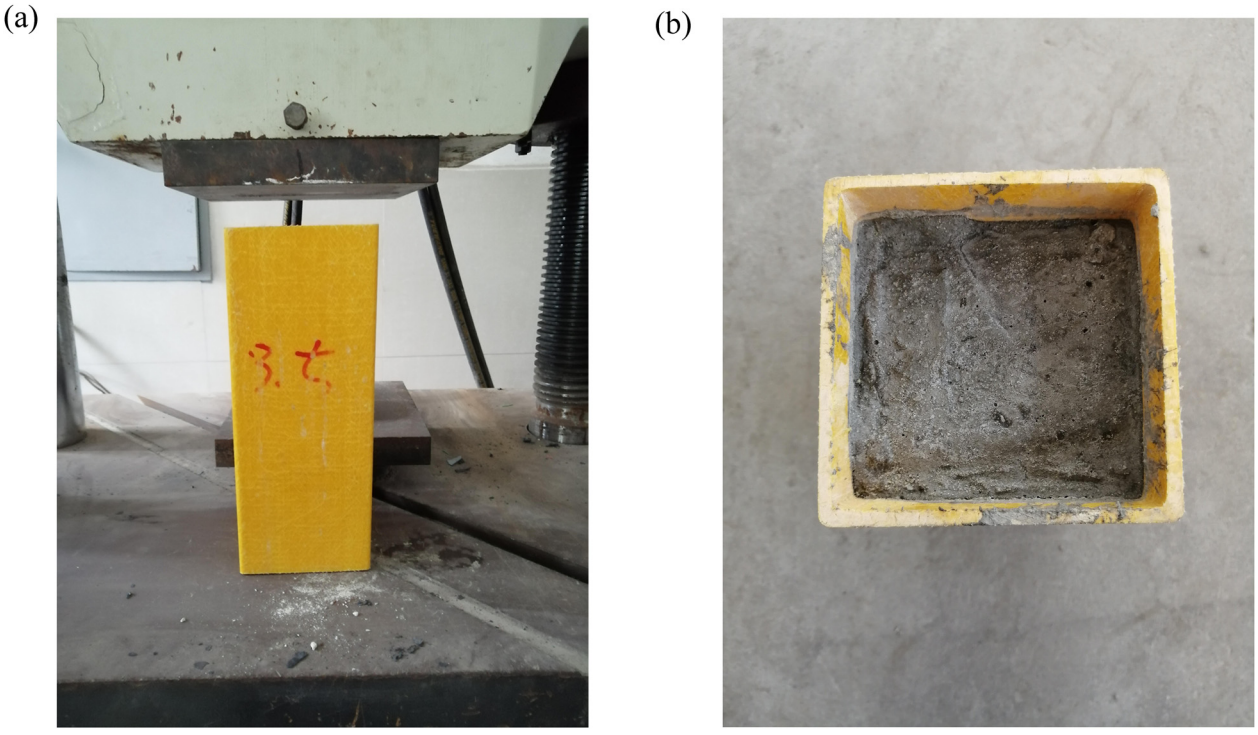

Figure 1: Pictures of the specimen: (a) elevation view and (b) overhead view.

Table 2: Material properties of the GFRP tube

Tensile direction	E_G (MPa)	f_{yG} (MPa)	f_{uG} (MPa)	f_{ay} (MPa)	f_{au} (MPa)
Transverse	8.3	133.4	32.4	241.35	340.5
Longitudinal	41.6	349.7	648.6		

Shaikh and Supit [16] showed that when the content of nano-$CaCO_3$ is 1%, the mechanical behavior of the concrete was greatly improved. Therefore, the concrete mixed with 1% nano-$CaCO_3$ was used to fill the GFRP tube in the experiment. Due to the large specific surface area and strong surface activity of nanomaterials, it is easy to agglomerate into larger particle size agglomerate particles and flocculent particles in the process of use, which can affect the performance of nanomaterials and reduce their purpose of improving the performance of concrete. Therefore, the first step of the nano-concrete production is to mix a certain amount of nano-$CaCO_3$ with water to form a mixed solution. Then, the coarse aggregates, fine aggregates, and cementitious materials are added into the concrete mixer in turn to mix evenly, and finally, the mixed solution is poured into the concrete mixer to mix evenly to form the nano-$CaCO_3$ concrete. The macroscopic morphology of nano-$CaCO_3$ is displayed in Figure 2, and the electronic microscopic picture of the nano-$CaCO_3$ concrete is shown in Figure 3. Table 3 shows the mix proportion of the nano-$CaCO_3$ concrete. During the preparation of the nano-$CaCO_3$ concrete, a total of nine standard concrete blocks with the dimensions of 150 mm × 150 mm × 150 mm were cast for each strength grade (C20, C30, and C40) and then cured in the same conditions as the specimens [35,36]. After 28 days of curing, the concrete blocks were loaded in accordance with the Code for Design of Concrete Structure (GB50010-2010) [37]. The measured compressive strength of the concrete blocks is shown in Table 4, including the ultimate compressive strength (f_{cu1}, f_{cu2}, and f_{cu3}) and average compressive strength ($f_{cu,m}$).

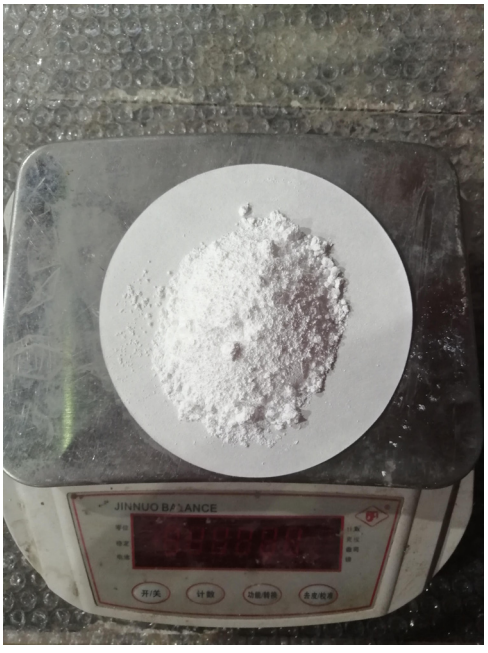

Figure 2: Nano-$CaCO_3$ powder.

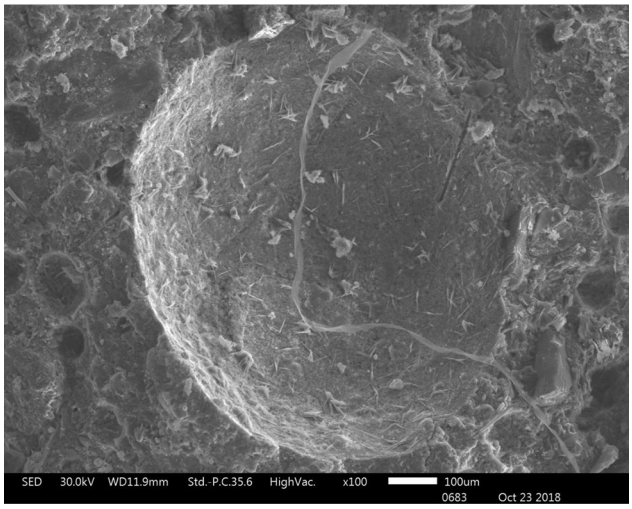

Figure 3: Scanning electron microscope picture of nano-$CaCO_3$ concrete.

2.3 Loading devices and schemes

The electro-hydraulic servo universal testing machine with a maximum range of 1,000 kN was utilized to load the specimens, as shown in Figure 4. Four repeated push-out tests were required for each specimen. In the experiment, the method of the monotonic hierarchical static loading was adopted, and the values of axial load and bond–slip were automatically monitored and recorded.

Before loading, it is necessary to adjust the base and keep the base parallel to the machine, then place a small cylindrical cushion block on the base, and place the specimen on the cylindrical cushion block to ensure that

Table 3: Mix proportions of the nano-$CaCO_3$ concrete

Design strength grade	Cement (kg m^{-3})	Fine aggregate (kg m^{-3})	Coarse aggregate (kg m^{-3})	Water (kg m^{-3})	Nano-$CaCO_3$ (kg m^{-3})
C20	350	690	1,160	185	3.5
C30	450	600	1,192	183	4.5
C40	520	525	1,220	178	5.2

Table 4: Mechanical properties of the nano-$CaCO_3$ concrete

Design strength grade	f_{cu1} (MPa)	f_{cu2} (MPa)	f_{cu3} (MPa)	$f_{cu,m}$ (MPa)
C20	28.3	29.5	27.4	28.4
C30	37.1	36.9	38.3	37.4
C40	46.3	47.4	46.1	46.6

the push-out tests can be carried out normally. In the first push-out test (forward direction), the specimen was loaded at a lower loading speed during the initial loading stage until the axial load–slip curve tended to be gentle, and then, the loading speed was increased. When the slip between the concrete in the GFRP tube and the GFRP tube reached the maximum value, the first push-out test was stopped. Then, the specimen was inverted, and the second push-out test (reverse direction) was carried out. When the slip between the concrete in the GFRP tube and the GFRP tube reached the maximum value, the second push-out test was stopped. Next, the specimen was inverted again, and the third push-out test (forward direction) was carried out. When the slip between the concrete in the GFRP tube and the GFRP tube reached the maximum value, the third push-out test was stopped. Finally, the specimen was inverted again, and the fourth push-out test (opposite direction) was carried out. The fourth push-out test was stopped when the slip between the concrete in the GFRP tube and the GFRP tube reached the maximum value. The loading diagram of the test specimens is shown in Figure 5.

Figure 4: Loading apparatus.

3 Experimental results and analysis

3.1 Loading process and phenomenon

A slight sound was produced during the loading process of the specimens, which was likely to be the friction sound caused by the slip between the inner concrete and the pultruded GFRP tube. When the load reached a certain level, the sound of “bang” was heard suddenly. This is the sound of the concrete being pushed out of the GFRP tube. At this time, it can be seen that the cushion block rose rapidly with the concrete, and the load began to decrease. Then, the load change was very small and the slip value increased all the time. Finally, the load suddenly increased again, indicating that the concrete in the GFRP tube was pushed to the top of the GFRP tube. At this point, the test was ended.

After the specimen was loaded, it was observed that there was no obvious change in the square GFRP tube, and the whole GFRP tube was intact without fracturing. However, the concrete in the square GFRP tube had the whole slip phenomenon. It can be found that the concrete surface in contact with square GFRP tube was slightly broken, but the whole concrete was relatively complete.

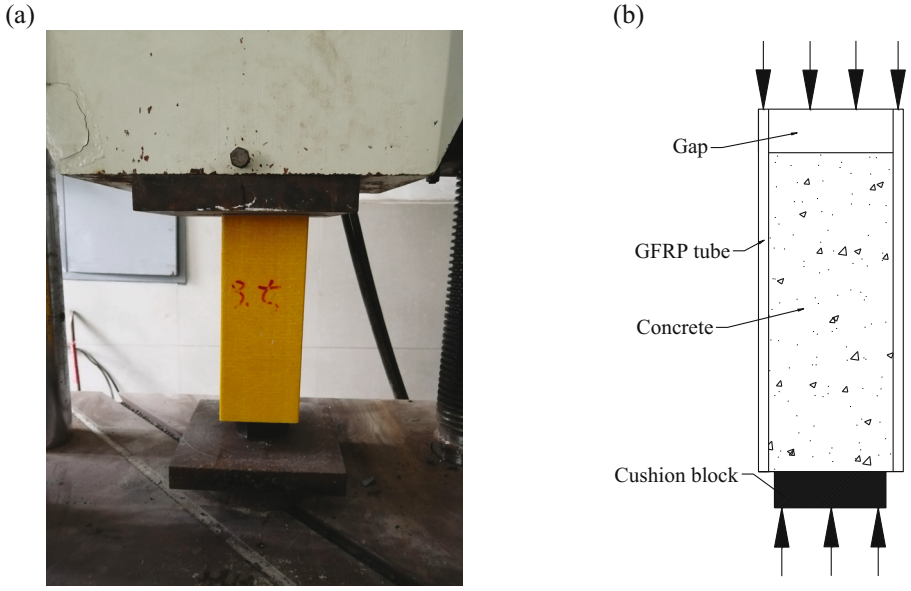

Figure 5: Loading diagram of the specimen: (a) loaded specimen and (b) diagrammatic sketch of loading.

There was a gap of 20–30 mm at the bottom of the GFRP tube initially filled with the concrete, and the gap between the concrete in the GFRP tube and the top of the GFRP tube was also reduced correspondingly. Then, the specimen was inverted and loaded again. In this way, the push-out test needed to be carried out four times. The first and the third push-out directions are the same, and the second and fourth push-out directions are the same. The damaged specimen is displayed in Figure 6.

3.2 Axial load–slip curves

Figure 7 shows the axial load–slip curves of each concrete-filled pultruded square GFRP column. Since four repeated push-out tests were carried out for each specimen, each specimen has four axial load–slip curves. The number after the label of each specimen in the legend refers to the number of push-out tests. For example, the last number "1" in "GT3.5-C20-1" refers to the first push-out test.

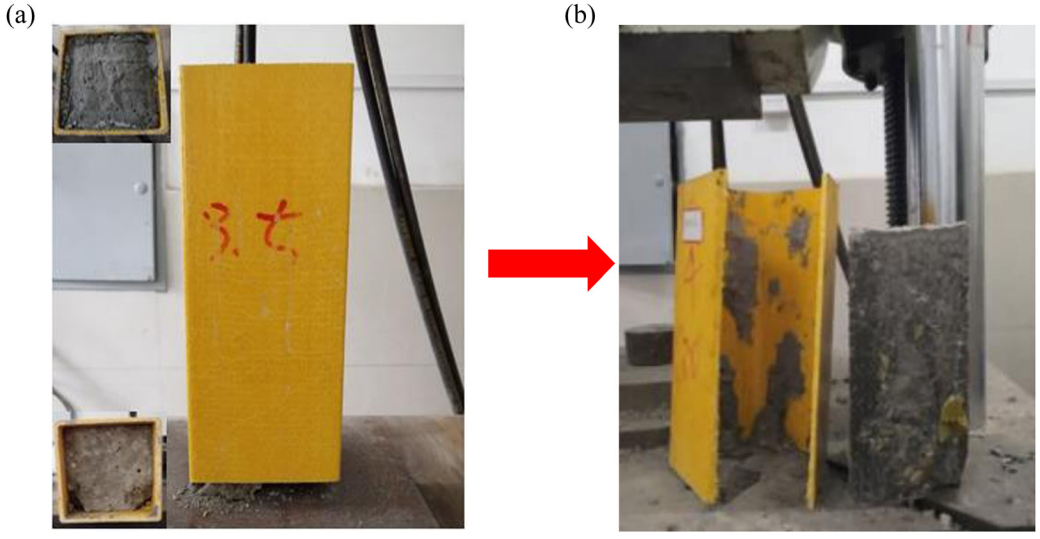

Figure 6: Failure process of specimens: (a) before loading and (b) after loading.

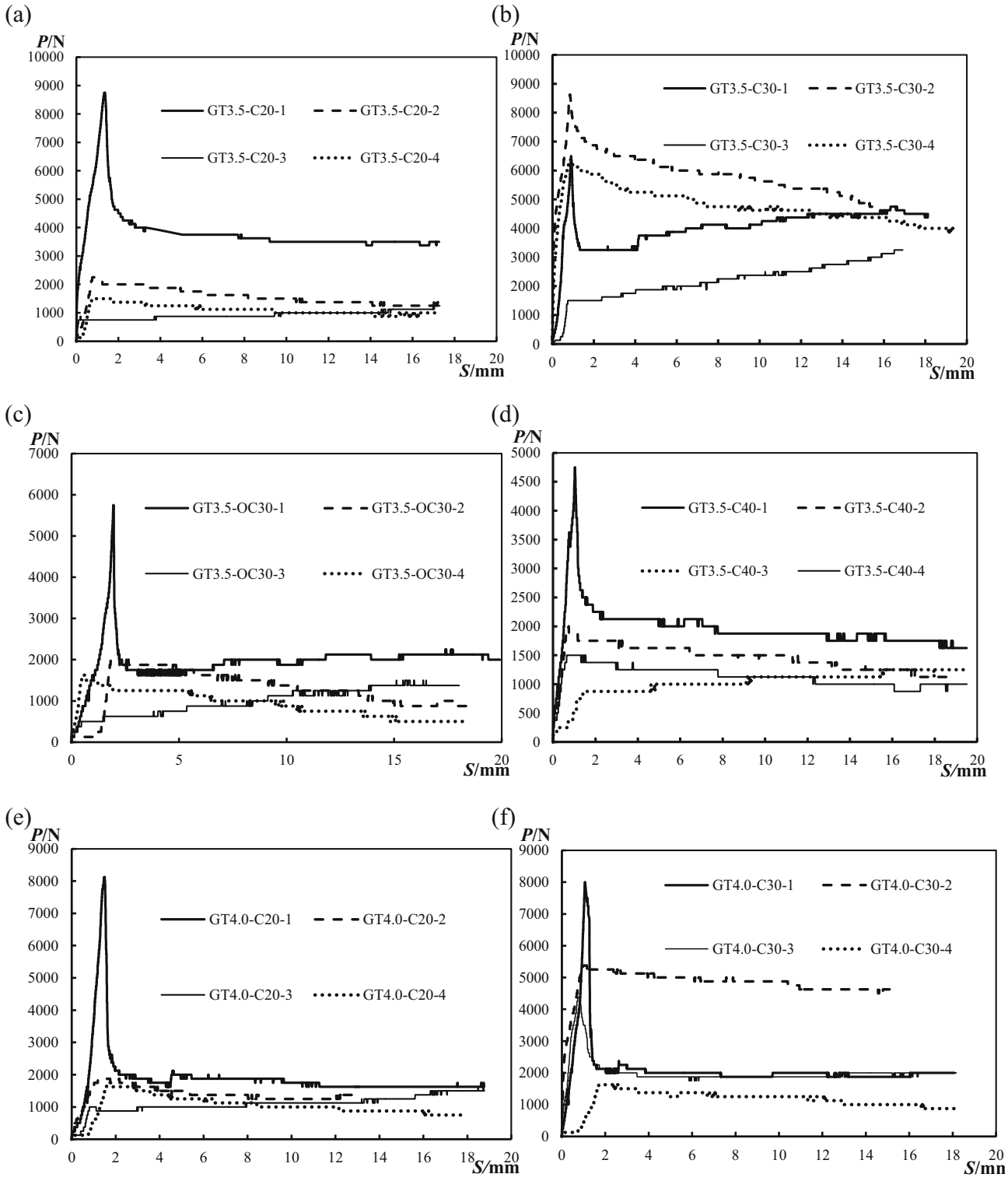

Figure 7: Continued

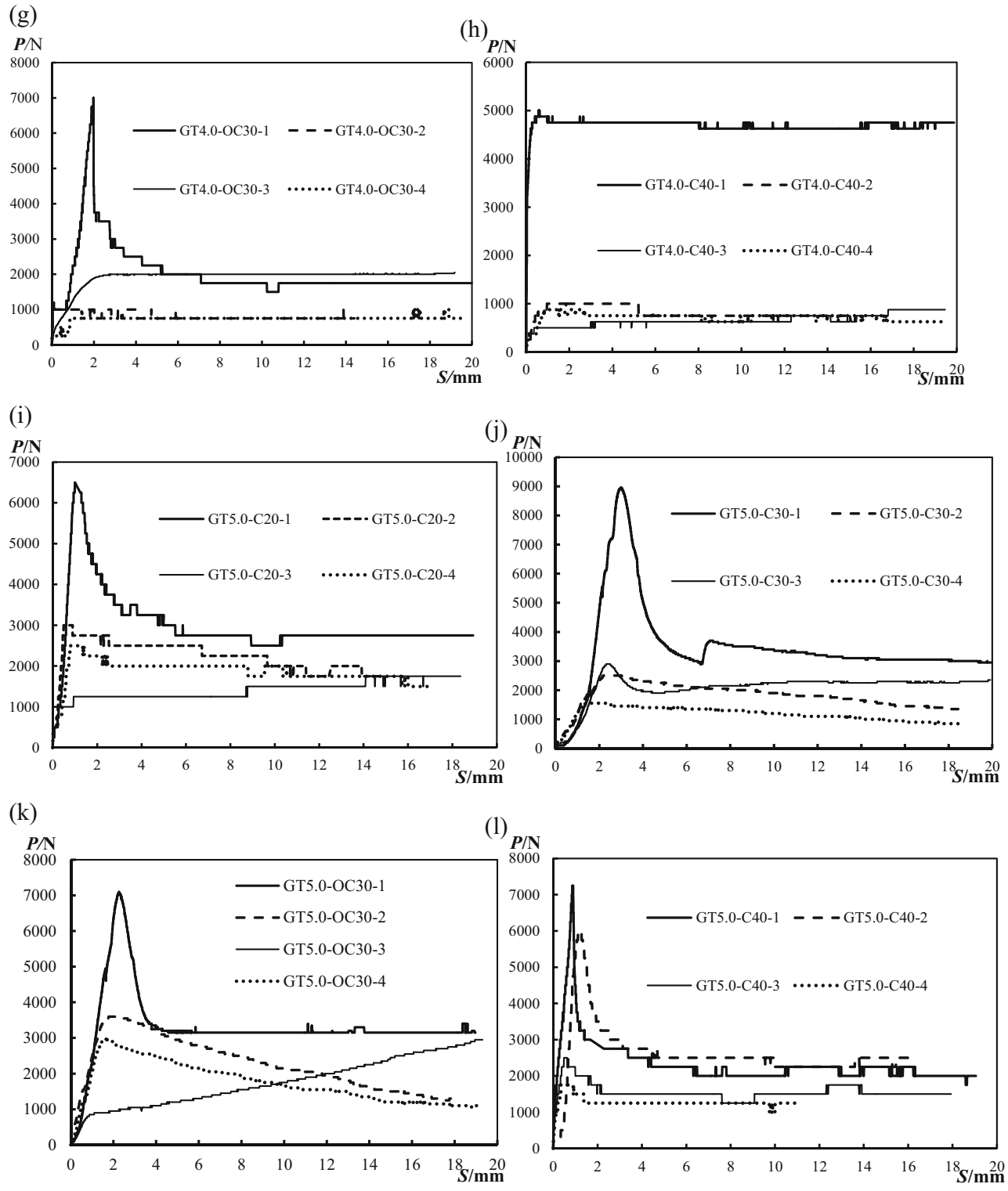

Figure 7: (a–l) Axial load–slip curves: (a) GT3.5-C20, (b) GT3.5-C30, (c) GT3.5-OC30, (d) GT3.5-C40, (e) GT4.0-C20, (f) GT4.0-C30, (g) GT4.0-OC30, (h) GT4.0-C40, (i) GT5.0-C20, (j) GT5.0-C30, (k) GT5.0-OC30, (l) GT5.0-C40.

Figure 7 shows two types of axial load–slip curves for each concrete-filled pultruded square GFRP column. There is a peak point for the first type of axial load–slip curve, while there is only an inflection point in the second type of axial load slip–curve and no peak point. Most of the axial load–slip curves of the first, second,

and fourth push-out tests belong to the first type, and the axial load–slip curves of the third push-out test basically belong to the second type. For the first type of axial load–slip curve, at the initial stage of loading, the curve generally shows a linear growth state. At this time, there is no relative slip between the GFRP tube and the concrete. Only the interface between the GFRP tube and the concrete at both ends of the specimen has a small slip, which indicates that the chemical bond action plays a role. With the increase of the load, the slip occurs in the concrete in the GFRP tube, the chemical bond action is lost, and the mechanical interlocking between the GFRP tube and the concrete starts to work. The subsequent curve continues to rise until the peak point is reached, but it is not linear. At this stage, the mechanical interlocking between the GFRP tube and the concrete plays a leading role. After the peak point, the curve begins to fall. The bonding force between the GFRP tube and the nano-$CaCO_3$ concrete is mainly borne by the friction. At the beginning of the decline, the load drops rapidly, and the slip value of the specimen is still very small. Then, the curve gradually becomes smooth, and the load drops slightly, but the slip value of the specimen is relatively large. Finally, the curve tends to be steady. Although the curve has a little shake, the load is roughly the same, and the slip value of the specimen increases all the time.

For the second type of axial load–slip curve, the rising stage of the curve is the same as that of the first type. As the load continues to rise, although the curve is always in the rising state, it does not reach the peak point as the first type, but there is an inflection point. After the inflection point, the curve does not decline, but it keeps in a stable state. Although the curve has a little shake, the load is nearly the same, and the slip value of the specimen increases all the time. However, there are also some curves showing an upward trend after the inflection point. At this time, the bonding force between the GFRP tube and the concrete is mainly borne by the friction.

3.3 Shear bond strength

The diagrammatic sketch of stress between the GFRP tube and the concrete in the GFRP tube during the push-out process is shown in Figure 8. The load is transferred between the GFRP tube and the concrete in the GFRP tube through the bond interface. A small segment δ in

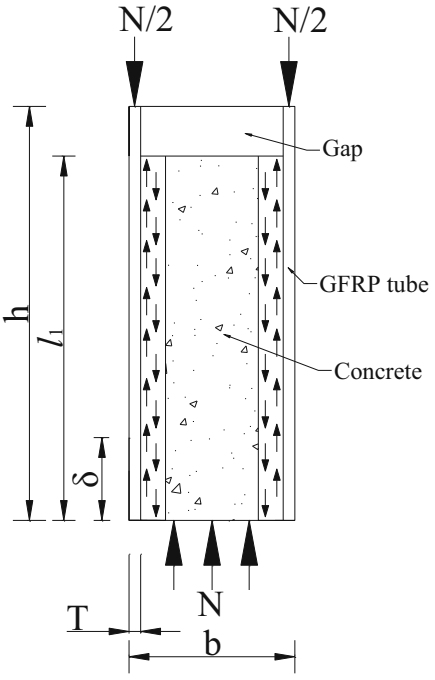

Figure 8: Diagrammatic sketch of stress of the specimen.

the GFRP column is taken, and the axial compressive strain of this segment is obtained by integration:

$$\varepsilon_\delta = \frac{\int_0^\delta 4b\tau(\delta)\mathrm{d}\delta}{4bTE_\mathrm{G}} = \frac{\int_0^\delta \tau(\delta)\mathrm{d}\delta}{TE_\mathrm{G}}. \tag{1}$$

It is assumed that the shear bond stress between the square GFRP tube and the concrete in the GFRP tube is uniformly distributed on the contact surface between the GFRP tube and the concrete [31]. Therefore, $\tau(\delta) = \tau$, and the formula for the shear bond strength between the square GFRP tube and the concrete is as follows:

$$\varepsilon = \frac{\int_0^{l_1} \tau\mathrm{d}\delta}{TE_\mathrm{G}} = \frac{\tau l_1}{TE_\mathrm{G}}, \tag{2}$$

$$\tau = N/4bl_1, \tag{3}$$

where T is the thickness of the GFRP tube; E_G is the elastic modulus of the GFRP tube; b is the side length of the GFRP tube; τ is the shear bond strength between the GFRP tube and the concrete; N is the ultimate bond failure load between the GFRP tube and the concrete, which is equal to the bond failure load in the first push-out test; and l_1 is the length of the contact surface

Table 5: Experimental results of specimens

Specimens	P_1 (N)	S_1 (mm)	τ (MPa)	P_2 (N)	P_3 (N)	P_4 (N)	f (N)	P_f (%)	P_1/P_3	P_2/P_4
GT3.5-C20	8,750	1.36	0.099	2,250	750	1,500	3,500	40	11.67	1.50
GT3.5-C30	6,500	0.90	0.074	8,625	1,500	6,375	4,500	69	4.33	1.35
GT3.5-OC30	5,750	1.95	0.065	4,000	500	2,875	2,125	37	11.50	1.39
GT3.5-C40	4,750	1.04	0.054	2,000	875	1,500	1,875	39	5.43	1.33
GT4.0-C20	8,125	1.48	0.092	1,875	1,000	1,750	1,625	20	8.13	1.15
GT4.0-C30	8,000	1.06	0.091	5,375	4,375	1,625	2,000	25	1.83	2.69
GT4.0-OC30	7,000	1.98	0.080	1,250	2,000	750	1,750	25	3.50	1.67
GT4.0-C40	5,000	1.99	0.056	1,000	500	875	4,625	93	10.00	1.14
GT5.0-C20	6,500	1.00	0.074	3,000	1,000	2,500	2,750	42	6.50	1.20
GT5.0-C30	8,950	2.96	0.102	2,500	2,900	1,550	3,000	34	3.09	1.61
GT5.0-OC30	7,100	2.24	0.081	3,900	900	3,000	3,150	44	1.82	1.30
GT5.0-C40	7,250	0.87	0.082	6,000	2,500	1,750	2,000	28	2.90	3.43

between the GFRP tube and the concrete. In Table 5, the bond strength between the square GFRP tube and the concrete is also calculated according to the aforementioned formula.

3.4 Comparison of the test results

Table 5 shows the test results, including the bond failure load (P_1, P_2, P_3, and P_4) of each specimen in four repeated push-out tests, bond failure slip (S_u), friction resistance (f), bond strength (τ), and the ratio of friction resistance to the first bond failure load (P_f). For the first type of axial load–slip curves, the bond failure load is the peak load. For the second type of axial load–slip curves, the corresponding load at the inflection point is the bond failure load. The bond failure slip (S_u) is the corresponding slip value when the applied load in the first push-out test reaches the bond failure load.

The first and the third push-out directions are the same, and the second and fourth push-out directions are the same. Therefore, for each specimen, the first bond failure load is compared with the third bond failure load, and the second bond failure load is compared with the fourth bond failure load. By comparison, it can be seen that the first bond failure load (P_1) of each specimen is greater than the third bond failure load (P_3), and the second bond failure load (P_2) of each specimen is greater than the fourth bond failure load (P_4). Therefore, for the push-out tests of each specimen in the same direction, with the increase in the number of push-out tests, the bond failure load of the specimen decreases. This is because with the increase in the number of push-out tests, the interface concrete is gradually crushed and ground up, which makes the mechanical interlocking between the GFRP tube and the concrete gradually weakened. The friction resistance in Table 5 is the last stable load in the first push-out test, and the ratio of friction resistance to the first bond failure load is mostly between 20% and 70%.

In addition, the test results show that the ultimate bond failure load between the GFRP tube and the nano-$CaCO_3$ concrete is larger than that between the GFRP tube and the ordinary concrete, as well as the bond failure slip between the GFRP tube and the nano-$CaCO_3$ concrete is smaller than that between the GFRP tube and the ordinary concrete. The bond strength between the GFRP tube and the nano-$CaCO_3$ concrete is 13.8% higher than that between the GFRP tube and the ordinary concrete when the GFRP tube thickness is 3.5 or 4.0 mm. The bond strength between the GFRP tube and the nano-$CaCO_3$ concrete is 26% higher than that between the GFRP tube and the ordinary concrete when the GFRP tube thickness is 5.0 mm. It can be concluded that the bond performance between the GFRP tube and the nano-$CaCO_3$ concrete is better than that between the GFRP tube and the ordinary concrete. This is because when the nano-$CaCO_3$ is added into the ordinary concrete, the bond performance between the core concrete and the GFRP tube is significantly increased owing to the tiny structural unit of the nano-$CaCO_3$ concrete.

3.5 Effect of concrete strength and GFRP tube thickness

Figure 9(a) shows the effect of nano-$CaCO_3$ concrete strength on the bond strength of specimens. It can be seen from Figure 9(a) that the bond strength of the specimen decreases with the increase in the nano-$CaCO_3$ concrete strength. When the GFRP tube thickness is 3.5 mm, the decrease percentage of bond strength is about 26% as the nano-$CaCO_3$ concrete strength increases from C20 to C40. When the GFRP tube thickness is 4.0 mm, the decrease

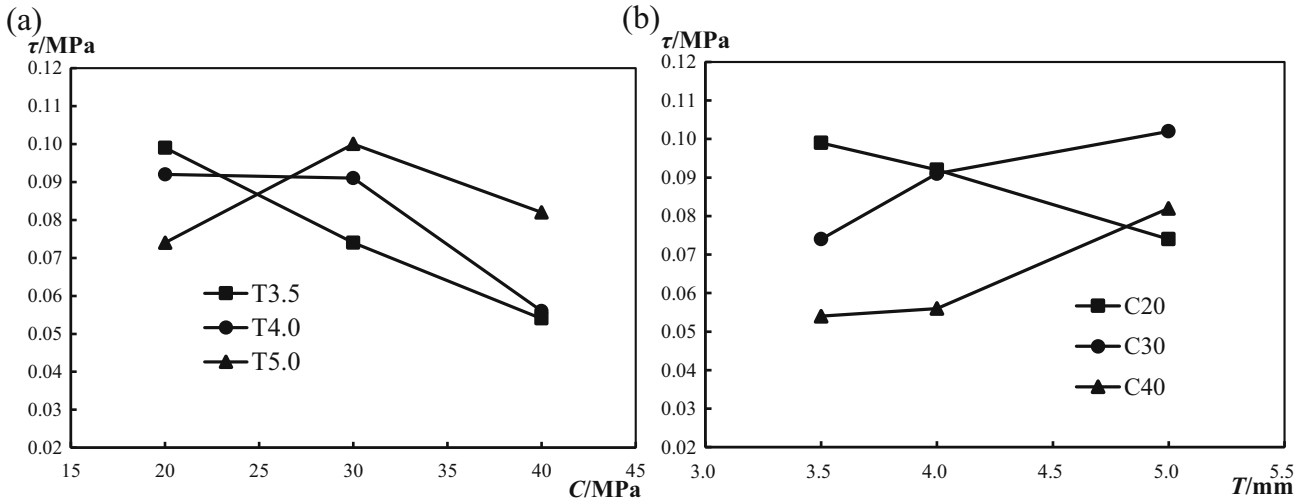

Figure 9: Effects of the (a) concrete strength and (b) GFRP tube thickness.

percentage of bond strength is about 20% as the nano-$CaCO_3$ concrete strength increases from C20 to C40. When the GFRP tube thickness is 5.0 mm, the decrease percentage of bond strength is about –9.5% as the nano-$CaCO_3$ concrete strength increases from C20 to C40. It can be seen from the decrease percentage of bond strength that this rule is obvious when the GFRP tube thickness is small (3.5 mm). With the increase in GFRP tube thickness, although there is a certain fluctuation, it generally follows this rule.

Figure 9(b) shows the effect of GFRP tube thickness on the bond strength of specimens. As shown in Figure 9(b), when the nano-$CaCO_3$ concrete strength is relatively small (C20), the bond strength of the specimen decreases as the GFRP tube thickness increases. When the nano-$CaCO_3$ concrete strength is C20, the decrease percentage of bond strength is about 13.5% as the GFRP tube thickness increases. When the nano-$CaCO_3$ concrete strength is relatively larger (C30 and C40), the bond strength of the specimen increases as the GFRP tube thickness increases. When the nano-$CaCO_3$ concrete strength is C30, the increase percentage of bond strength is about 26.5% as the GFRP tube thickness increases. When the nano-$CaCO_3$ concrete strength is C40, the increase percentage of bond strength is about 18% as the GFRP tube thickness increases.

4 Conclusions

In this study, a total of 12 specimens were designed, and four repeated push-out tests were carried out on each specimen to study the bond–slip performance between the pultruded GFRP tube and the nano-$CaCO_3$ concrete. The effects of nano-$CaCO_3$ concrete strength and thickness of GFRP tube on the bond strength of specimens were also analyzed and evaluated. Through the analyses of the experimental results, the following conclusions can be drawn:

(1) There are two types of axial load–slip curves for the concrete-filled pultruded GFRP column. The first type of axial load–slip curve has a peak point, while the second type of axial load–slip curve has an inflection point instead of the peak point. The axial load–slip curves of the first, second, and fourth push-out tests generally belong to the first type, while the axial load–slip curves of the third push-out tests basically belong to the second type.
(2) Comparison of the results of the push-out tests of each specimen in the same direction shows that the bond failure load of the specimen decreases with the increase in the number of push-out tests. This is because the concrete is gradually crushed and ground with the increase in the number of push-out tests.
(3) The ultimate bond failure load between the GFRP tube and the nano-$CaCO_3$ concrete is larger than that between the GFRP tube and the ordinary concrete. The bond failure slip value between the GFRP tube and the nano-$CaCO_3$ concrete is smaller than that between the GFRP tube and the ordinary concrete.
(4) The bond strength of the specimen decreases with the increase in the nano-$CaCO_3$ concrete strength. When the thickness of GFRP tube is relatively small (3.5 mm), the decrease percentage of bond strength is more obvious.

(5) When the nano-$CaCO_3$ concrete strength is relatively small (C20), the bond strength of the specimen decreases with the increases in the GFRP tube thickness. However, when the nano-$CaCO_3$ concrete strength is relatively larger (C30 and C40), the bond strength of the specimen is increased with the increase in the GFRP tube thickness.

5 Nomenclature

b	side length of the GFRP tube
E_G	elastic modulus of the GFRP tube
f	friction resistance
f_{au}	average tensile strength of the GFRP tube
f_{ay}	average yield strength of the GFRP tube
f_c	strength grade of the concrete
f_{cu}	average compressive strength of the nano-$CaCO_3$ concrete
f_u	tensile strength of the GFRP tube
f_y	yield strength of the GFRP tube
h	height of the specimen
l_1	length of the contact surface between the GFRP tube and the concrete
N_u	ultimate bond failure load
P_1	bond failure load of the first push-out test
P_2	bond failure load of the second push-out test
P_3	bond failure load of the third push-out test
P_4	bond failure load of the fourth push-out test
P_f	ratio of friction resistance to the first bond failure load
S_u	bond failure slip
τ	bond strength

Acknowledgment: The authors thank the support of the National Natural Science Foundation of China (No. 51778066).

Conflict of interest: The authors declare no conflict of interest regarding the publication of this paper.

References

[1] Zhuang CL, Chen Y. The effect of nano-SiO_2 on concrete properties: a review. Nanotechnol Rev. 2019;8:562–72.
[2] Li ZH, Xu K, Wei F. Recent progress in photodetectors based on low-dimensional nanomaterials. Nanotechnol Rev. 2018;7:393–411.
[3] Pawłowski R, Pawłowski B, Wita H, Pluta A, Sobik P, Sala A, et al. Silver nanoparticles in the thermal silver plating of aluminium busbar joints. Nanotechnol Rev. 2018;7:365–72.
[4] Das S, Ghosh CK, Sarkar CK, Roy S. Facile synthesis of multi-layer graphene by electrochemical exfoliation using organic solvent. Nanotechnol Rev. 2018;7(6):497–508.
[5] Zeidan M, Said AM. Effect of colloidal nano-silica on alkalisilica mitigation. J Sustainable Cem-Based Mater. 2017;6:126–38.
[6] Kontoleontos F, Tsakiridis PE, Marinos A, Kaloidas V, Katsioti M. Influence of colloidal nanosilica on ultrafine cement hydration: Physicochemical and microstructural characterization. Constr Build Mater. 2012;35:347–60.
[7] Gupta M, Kumar M. Effect of nano silica and coir fiber on compressive strength and abrasion resistance of concrete. Constr Build Mater. 2019;226:44–50.
[8] Zhang MH, Islam J, Peethamparan S. Use of nano-silica to increase early strength and reduce setting time of concretes with high volumes of slag. Cem Concr Compos. 2012;34:650–62.
[9] Sun XJ, Zhang H, Meng WJ, Zhang RH, Li KN, Peng T. Primary resonance analysis and vibration suppression for the harmonically excited nonlinear suspension system using a pair of symmetric viscoelastic buffers. Nonlinear Dynam. 2018;94:1243–65.
[10] Guo K, Miao H, Liu L, et al. Effect of graphene oxide on chloride penetration resistance of recycled concrete. Nanotechnol Rev. 2019;8:681–9.
[11] Pacheco-Torgal F, Miraldo S, Ding Y, Labrincha JA. Targeting HPC with the help of nanoparticles: An overview. Constr Build Mater. 2013;38:365–70.
[12] Lin QJ, Chen Y, Liu C. Mechanical properties of circular nano-silica concrete filled stainless steel tube stub columns after being exposed to freezing and thawing. Nanotechnol Rev. 2019;8:600–18.
[13] He K, Chen Y, Xie WT. Test on axial compression performance of nano-silica concrete-filled angle steel reinforced GFRP tubular column. Nanotechnol Rev. 2019;8:523–38.
[14] Behfarnia K, Salemi N. The effects of nano-silica and nano-alumina on frost resistance of normal concrete. Constr Build Mater. 2013;48:580–4.
[15] Shaikh FUA, Supit SWM. Chloride induced corrosion durability of high volume fly ash concretes containing nano particles. Constr Build Mater. 2015;9:208–25.
[16] Shaikh FUA, Supit SWM. Mechanical and durability properties of high volume fly ash (HVFA) concrete containing calcium carbonate ($CaCO_3$) nanoparticles. Constr Build Mater. 2014;70:309–21.
[17] Liu XY, Chen L, Liu AH, Wang XR. Effect of nano-$CaCO_3$ on properties of cement paste. Energy Procedia. 2012;16:991–6.
[18] Mirmiran A, Shahawy M. A new concrete-filled hollow FRP composite column. Compos Part B Eng. 1996;27:263–8.
[19] Mirmiran A, Samaan M, Cabrera S, Shahawy M. Design, manufacture and testing of a new hybrid column. Constr Build Mater. 1998;12:39–49.
[20] Yu T, Hu YM, Teng JG. FRP-confined circular concrete-filled steel tubular columns under cyclic axial compression. J Constr Steel Res. 2014;94:33–48.
[21] Zhang Y, Zhang LW, Liew KM, Yu JL. Buckling analysis of graphene sheets embedded in an elastic medium based on

the kp-Ritz method and non-local elasticity theory. Eng Anal Bound Elem. 2016;70:31–93.
[22] Singh SB, Vummadisetti S, Chawla H. Influence of curing on the mechanical performance of FRP laminates. J Build Eng. 2018;16:1–19.
[23] Robert M, Benmokrane B. Combined effects of saline solution and moist concrete on long-term durability of GFRP reinforcing bars. Constr Build Mater. 2013;38:274–84.
[24] Al-Salloum YA, El-Gamal S, Almusallam TH, Alsayed SH, Aqel M. Effect of harsh environmental conditions on the tensile properties of GFRP bars. Compos Part B Eng. 2013;45(1):835–44.
[25] Liao K, Schultheisz CR, Hunston DL. Effects of environmental aging on the properties of pultruded GFRP. Compos Part B Eng. 1999;30:485–93.
[26] Zhang RH, He ZC, Wang HW, Wang HW, You F, Li KN. Study on self-tuning tyre friction control for developing main-servo loop integrated chassis control system. IEEE Access. 2017;5: 6649–60.
[27] Gooranorimi O, Suaris W, Nanni A. A model for the bond-slip of a GFRP bar in concrete. Eng Struct. 2017;146: 34–42.
[28] Gooranorimi O, Claure G, Suaris W, Nanni A. Bond-slip effect in flexural behavior of GFRP RC slabs. Compos Struct. 2018;193:80–86.
[29] Yuan H, Lu XS, Hui D, Feo L. Studies on FRP-concrete interface with hardening and softening bond-slip law. Compos Struct. 2012;94:3781–92.
[30] Vilanova I, Torres L, Baena M, Liorens M. Numerical simulation of bond-slip interface and tension stiffening in GFRP RC tensile elements. Compos Struct. 2016;153:504–13.
[31] Tekle BH, Khennane A, Kayali O. Bond behavior of GFRP reinforcement in alkali activated cement concrete. Constr Build Mater. 2017;154:972–82.
[32] Yuan JS, Hadi MNS. Bond-slip behavior between GFRP I-section and concrete. Compos Part B Eng. 2017;130:76–89.
[33] Lu XZ, Teng JG, Ye LP, Jiang JJ. Bond-slip models for FRP sheets/plates bonded to concrete. Eng Struct. 2005;27:920–37.
[34] ASTM D3039/D3039M-08, Standard test method for tensile properties of polymer matrix composite materials, West Conshohocken, PA, 2008.
[35] JGJ 52-2006, Standard for technical requirements and test method of sand and crushed stone (or gravel) for ordinary concrete, China Architecture and Building Press, Beijing China, 2006. (In Chinese).
[36] GB 50204-2002, Code for Construction Acceptance of Concrete Structure Engineering, China Architecture and Building Press, Beijing China, 2002. (In Chinese).
[37] GB 50010-2010, Code for Design of Concrete Structures, China Architecture and Building Press, Beijing China, 2010. (In Chinese).